

Fully relativistic energies, transition properties, and lifetimes of lithium-like germanium

Shuang Li(李双), Jing Zhou(周璟), Liu-Hong Zhu(朱柳红), Xiu-Fei Mei(梅秀菲), and Jun Yan(颜君)

Citation: Chin. Phys. B, 2024, 33 (**10**): 103102. DOI: 10.1088/1674-1056/ad7c30
Journal homepage: http://cpb.iphy.ac.cn; http://iopscience.iop.org/cpb

What follows is a list of articles you may be interested in

Low-lying electronic states of osmium monoxide OsO

Wen Yan(严汶) and Wenli Zou(邹文利)
Chin. Phys. B, 2023, 32 (**11**): 113101. DOI: 10.1088/1674-1056/acec46

Fully relativistic many-body perturbation energies, transition properties, and lifetimes of lithium-like iron Fe XXIV

Shuang Li(李双), Min Zhao(赵敏), Guo-Qing Liu(刘国庆), Chang-Bao Hu(胡昌宝), and Guo-Zhu Pan(潘国柱)
Chin. Phys. B, 2023, 32 (**10**): 103101. DOI: 10.1088/1674-1056/acef01

Theoretical study on the transition properties of AlF

Yun-Guang Zhang(张云光), Ling-Ling Ji(吉玲玲), Ru Cai(蔡茹),Cong-Ying Zhang(张聪颖), and Jian-Gang Xu(徐建刚)
Chin. Phys. B, 2022, 31 (**5**): 053101. DOI: 10.1088/1674-1056/ac3648

Highly accurate theoretical study on spectroscopic properties of SH including spin-orbit coupling

Shu-Tao Zhao(赵书涛), Xin-Peng Liu(刘鑫鹏), Rui Li(李瑞), Hui-Jie Guo(国慧杰), and Bing Yan(闫冰)
Chin. Phys. B, 2021, 30 (**7**): 073104. DOI: 10.1088/1674-1056/ac003f

Vibronic spectra of aluminium monochloride relevant to circumstellar molecule

Jian-Gang Xu(徐建刚), Cong-Ying Zhang(张聪颖), Yun-Guang Zhang(张云光)
Chin. Phys. B, 2020, 29 (**3**): 033102. DOI: 10.1088/1674-1056/ab6c46

DATA PAPER

Fully relativistic energies, transition properties, and lifetimes of lithium-like germanium

Shuang Li(李双)[1,2,3], Jing Zhou(周璟)[1], Liu-Hong Zhu(朱柳红)[1], Xiu-Fei Mei(梅秀菲)[1], and Jun Yan(颜君)[2,†]

[1] *School of Electrical and Optoelectronic Engineering, West Anhui University, Lu'an* 237012, *China*
[2] *Institute of Applied Physics and Computational Mathematics, Beijing* 100088, *China*
[3] *Shanghai EBIT Laboratory, Institute of Modern Physics, Department of Nuclear Science and Technology, Fudan University, Shanghai* 200433, *China*

(Received 8 August 2024; revised manuscript received 12 September 2024; accepted manuscript online 18 September 2024)

Employing two fully relativistic methods, the multi-reference configuration Dirac–Hartree–Fock (MCDHF) method and the relativistic many-body perturbation theory (RMBPT) method, we report energies and lifetime values for the lowest 35 energy levels of the $(1s^2)nl$ configurations (where the principal quantum number $n = 2$–6 and the angular quantum number $l = 0, \ldots, n-1$) of lithium-like germanium (Ge XXX), as well as complete data on the transition wavelengths, radiative rates, absorption oscillator strengths, and line strengths between the levels. Both the allowed (E1) and forbidden (magnetic dipole M1, magnetic quadrupole M2, and electric quadrupole E2) ones are reported. The results from the two methods are consistent with each other and align well with previous accurate experimental and theoretical findings. We assess the overall accuracies of present RMBPT results to be likely the most precise ones to date. The present fully relativistic results should be helpful for soft x-ray laser research, spectral line identification, plasma modeling and diagnosing. The datasets presented in this paper are openly available at https://doi.org/10.57760/sciencedb.j00113.00135.

Keywords: multi-reference, Dirac–Hartree–Fock, relativistic many-body perturbation, radiative rate, lifetime

PACS: 31.15.vj, 31.15.am, 31.15.xp, 32.70.Cs **DOI:** 10.1088/1674-1056/ad7c30

1. Introduction

In recent years, there has been significant interest in lithium-like (Li-like) ions.[1–10] Studying these ions is crucial for exploring fundamental physics, including quantum electrodynamic (QED) effects.[1,2,4,5] Moreover, the relatively simple electronic structure of these ions allows for the theoretical generation of accurate spectral data, which further can be used in a budget-friendly approach to explore the nuclear properties.[11] These data are also valuable for spectral calibration, identification of spectral lines,[12] and diagnostics related to electron temperature, density, and chemical composition.[13–15]

Additionally, the Li-like aluminum ion Al^{10+} has been studied as the gain medium for a recombination plasma soft x-ray laser. Researchers have investigated the 3d–4f transition (wavelength: 15.47 nm) as a laser transition and obtained a gain coefficient of 9.84 cm^{-1}.[16] In plasma soft x-ray laser research, both wavelengths and lifetimes are crucial parameters.

On the experimental side, the spectra of Li-like ions have been extensively observed in both astrophysical and laboratory plasmas, as noted in references.[13–15] For instance, the spectra of lithium-like ions have been detected in various environments, including the solar corona,[17,18] laser-produced plasma,[19,20] tokamaks,[21,22] and electron beam ion traps.[23,24] Moreover, the spectra of lithium-like iron have been observed up to high levels with $n = 6$, as noted in references.[18,19,24]

On the theoretical side, it has been believed that there are only three electrons outside, the lithium-like ions with a simple structure and belonging to the few-body problem. For example, Yan and Drake have already provided high-precision theoretical results for lithium-like ions using the Hylleraas-type variational method.[25] However, the results are limited to the $n = 2$ level. Furthermore, the results are only semi-relativistic rather than fully relativistic, so the accuracy of the results will be significantly compromised for high-Z ions, such as the present case $Z = 32$, where relativistic effects are pronounced.

In fact, there have been many other theoretical studies on Li-like ions.[3,12–15,26–40] In particular, those involving Li-like germanium ($Z = 32$) are semi-empirical extrapolation method of Vainshtain and Safronova,[41] semi-relativistic research of Liang and Badnell,[15] and three fully relativistic research of Zhang *et al.*,[42] Johnson *et al.*,[43] and Khatri *et al.*[44]

The semi-empirical extrapolation method of Vainshtain and Safronova[41] utilized the perturbation method by power series $1/Z$ and αZ to provide energies for levels of $n \leq 5$ configurations for Li-like ions with $Z = 6$–42. However, the 4f, 5f, and 5g levels are missing, and the accuracy of the energies for the $2p_{1/2,3/2}$ levels is relatively poor, with differences of

†Corresponding author. E-mail: yan_jun@iapcm.ac.cn

© 2024 Chinese Physical Society and IOP Publishing Ltd

0.1% compared to NIST experimental ones.[45] Additionally, no radiative rates are reported, thus making it impossible to calculate the lifetimes.

Using the Autostructure program,[46] which is based on the Thomas–Fermi–Dirac–Amaldi model potential, Liang and Badnell[15] provided energy levels up to $n \leq 5$ and radiative rates for Li-like ions with $Z = 4$–36. In this semi-relativistic approach, relativistic effects were incorporated perturbatively using only the one-body Breit–Pauli operator (including mass–velocity, spin–orbit, and Darwin terms) without considering valence-electron two-body fine-structure operators. Compared to experimental energies from NIST,[45] there are significant deviations. For instance, the deviations for the $3s_{1/2}$, $3p_{1/2}$, $3d_{5/2}$, and $4d_{5/2}$ levels exceed 0.1%, and for the $2p_{3/2}$ level, the deviation can be as high as 0.8%. Although Liang and Badnell[15] presented transitions rates between levels up to $n \leq 5$, the lack of fully relativistic treatment results in significant differences in radiative rates compared to the fully relativistic results of Zhang *et al.*[42] For example, discrepancies for transitions such as $2p_{1/2}$–$3s_{1/2}$, $2p_{1/2}$–$4s_{1/2}$ are approximately 9% and 42%, respectively, while the discrepancy for the $2p_{1/2}$–$5s_{1/2}$ transition can be even as large as by a factor of 3.6. These discrepancies significantly impact the accuracy of the lifetimes deduced from Liang and Badnell.[15]

Based on the fully relativistic Dirac-Fock-Slater central potential, Zhang *et al.*,[42] provided energy levels up to $n = 5$ and a portion of E1 oscillator strengths (from which radiative rates can be derived) for Li-like ions with $Z = 8$–92, the provided oscillator strengths only involve the three lowest levels, $2s_{1/2}$, $2p_{1/2}$, and $2p_{3/2}$ as the lower level of a transition, thus many radiative decay channels from upper levels are not reported, making it impractical to calculate lifetimes for higher levels. Moreover, radiative decay channels from the 4f, 5f, and 5g levels are entirely missing. The lack of radiative decay channels from the 4f level particularly hampers the study of laser transition 3d–4f in Li-like ions.[16] Additionally, many energy levels with $n \geq 3$ show discrepancies of over 0.1% compared to experimental values from NIST,[45] including levels such as $3s_{1/2}$, $3p_{1/2}$, $3p_{3/2}$, $4d_{3/2}$, and $4d_{5/2}$.

Johnson *et al.*[43] employed fully relativistic third-order many-body perturbation theory to provide accurate energies and E1 radiative rates of Li-like ions with $Z = 3$–100. However, their data is limited to only the four lowest levels of the $nl \leq 3s_{1/2}$ configurations.

Khatri *et al.*[44] utilized the fully relativistic multi-reference configuration Dirac–Hartree–Fock (MCDHF) method to provide the energies of the eight lowest levels with $n \leq 3$ configurations and some, but not all, E1 radiative rates for Li-like ions with $Z = 32$, 36, 42, 46, 50, 54, and 56. However, the accuracy of the energies for the two $2p_{1/2,3/2}$ levels is poor, showing deviations of 0.1% compared to NIST experimental values.[45] Additionally, the missing of E1 radiative rates for the $2p_{3/2}$–$3d_{3/2}$ transition could lead to significant errors in the lifetime of the $3d_{3/2}$ level, which is the lower level of the important 3d–4f laser transition.[16]

Based on the above analyses, it is clear that only a few low-energy levels of Ge XXX have been accurately studied in previous experimental and theoretical researches. To provide comprehensive accurate energies, radiative properties, and lifetimes for the lowest 35 energy levels from $1s^2nl$ configurations with $n \leq 6$ and $l \leq n-1$ for Ge XXX, this study employs two fully relativistic approaches, the first approach is the multi-reference configuration Dirac–Hartree–Fock (MCDHF) method, as implemented in the GRASP2K code (version 2018[47]), the second is the relativistic many-body perturbation theory (RMBPT), as implemented in the FAC code.[48] The radiative properties provided include transition wavelengths, radiative rates, absorption oscillator strengths, and line strengths for both allowed (E1) and forbidden transitions (magnetic dipole M1, magnetic quadrupole M2, and electric quadrupole E2). In recent years, we have successfully applied both the approaches to achieve high accuracy in studying Li-like, O-like, F-like, Ne-like, and Ni-like ions.[7,49–52] This study is also a continuation of our work on Li-like isoelectronic sequences,[7] where we have reported fully relativistic energies, transition properties, and lifetimes of lithium-like iron.

Compared to existing theoretical studies, both our fully relativistic approaches consider the Breit interactions, the leading QED effects (vacuum polarization and self-energy), and detailed electron correlation effects. Consequently, we offer more accurate and comprehensive energies, radiative data, and lifetime values for more levels with $n \leq 6$.

2. Calculations

2.1. MCDHF

In this work, we use the MCDHF method as implemented in the GRASP2K code (version 2018[47]). Details of the method can be found in the references.[53–55] The GRASP2K code has also been used in our recent studies.[7,49–52] For brevity, only the computational procedures are described here.

We consider $(1s^2)nl$ configurations with $n \leq 6$ and $l \leq (n-1)$ as the multireference (MR). For even parity, 2s, 3s, 3d, 4s, 4d, 5s, 5d, 5g, 6s, 6d, and 6g are the nl. For odd parity, 2p, 3p, 4p, 4f, 5p, 5f, 6p, 6f, and 6h are the nl. We treat the $1s^2$ electrons as the core (C) and the nl electron as the valence (V).

Firstly, the orbitals with $n \leq 6$ from the above MR configurations are computed simultaneously using the extended optimal level (EOL) mode[55] in the Dirac–Hartree–Fock (DHF) calculations.

Secondly, during the self-consistent field (SCF) calculation, single (S) and double (D) substitutions are allowed for

all the $1 \le n \le 6$ electrons of the MR into the active set (AS) orbitals as follows:

$$\begin{aligned}
&\text{AS1} = \{7s,7p,7d,7f,7g,7h,7i\},\\
&\text{AS2} = \text{AS1}+\{8s,8p,8d,8f,8g,8h\},\\
&\text{AS3} = \text{AS2}+\{9s,9p,9d,9f,9g,9h\},\\
&\text{AS4} = \text{AS3}+\{10s,10p,10d,10f,10g\},\\
&\text{AS5} = \text{AS4}+\{11s,11p,11d,11f\},\\
&\text{AS6} = \text{AS5}+\{12s,12p,12d,12f\}. \qquad (1)
\end{aligned}$$

However, we restrict the double (D) substitution of the 1s core to the active set (AS) of {6s, 6p, 6d, 6f, 6g, 6h} for convergence requirement. To accelerate the SCF calculation, we only keep the configurations that interact with the MR. The AS is expanded layer by layer, allowing us to monitor the convergence of the results. At each step, only the newly added layer of orbitals is optimized, while the previously ones remain fixed. As the AS5 expands to the AS6 layer, the change in energies is less than 0.003% for all the $n \le 6$ levels, indicating that the convergence has been achieved.

For accurate atomic structure calculations, it is generally necessary to carefully consider the Breit interaction, the leading QED effects (including self-energy and vacuum polarization), the nuclear motion correction, as well as electronic correlation effects. Our researches show that the contribution of the Breit interaction to the absolute energy (not the excitation energy) of each level is always positive, ranging from +11.3 eV to +13.4 eV, and contributing around +11.3 eV for most levels, making the Breit interaction significant. Compared to the other levels, the Breit interaction has a relatively larger contribution to the *n*s and *n*p levels, and this contribution gradually decreases as *n* increases.

We further study on the leading quantum electrodynamics (QED) effects, which include the self-energy (SE) and vacuum polarization (VP) effects. Our researches show that the SE effect, with the contribution to the absolute energy ranging from +16.9 eV to +18.1 eV, contributes positively to all the levels and is roughly an order of magnitude larger than the VP effect, which is negative for all the levels, and the maximum VP contribution is around −1.8 eV. Thus, while both the SE and VP are significant, the overall QED effects in the present case are primarily driven by the SE effect. Specifically, the SE contribution is around +17 eV for most levels, but it is somewhat larger for the *n*s levels, with the contribution decreasing as *n* grows.

Regarding the nuclear motion correction to the absolute energy, our RMBPT tests (detailed in the next section) indicate that it is approximately 0.2 eV for all levels with $n \le 6$. However, as for the excitation energy, the correction is merely around 0.02 eV, which is negligible.

Thus in our final relativistic configuration interaction (RCI) calculations, the Breit interaction is incorporated through the transverse photon interactions at low frequencies by multiplying the frequency by a scale factor (typically set to 1.0×10^{-6}, as in the present case). We also account for the leading QED effects (SE and VP). However, we omit the nuclear motion correction. Meanwhile, in the final RCI calculations, we generate more configuration state functions (CSFs) through single (S), double (D), and triple (T) substitutions from the MR to the AS6. The needed orbitals are obtained from the previous SCF calculation of the AS6 layer and apply variational optimization only to the coefficients of the configurations.

2.2. RMBPT

To further evaluate the accuracy of the current MCDHF results, we also perform fully relativistic RMBPT calculations using the well-known flexible atomic code (FAC).[48] Detailed descriptions of the RMBPT method can be found in references,[37,56–58] so we will not delve into the theoretical details here. Instead, we provide an overview of the parameter settings.

In the present RMBPT computations, the Hilbert space is partitioned into two subspaces: the model space M (handling configuration interaction effects precisely) and the orthogonal space N (addressing configuration interaction effects through second-order perturbation). The M space incorporates all levels from the $(1s^2)nl$ configurations (where n, the principal quantum number, ranges from 2 to 8, and l, the angular quantum number, varies from 0 to $n-1$). The orthogonal space N includes all the single (S) and double (D) substitutions from the M space, with the highest S-substitutions extending to $n = 200$ and the highest D-substitutions involving the first and second electrons up to $n = 200$ and $n' = 65$, respectively. We also account for various corrections, including the Breit interaction, vacuum polarization (VP), and electron self-energy (SE) effects. Since our RMBPT test calculations have already incorporated the nuclear motion correction, our final RMBPT results reflect this adjustment, even though its effect is negligible.

2.3. Transition properties

The three transition properties: radiative transition rate (A in unit s^{-1}), absorption oscillator strength (f, dimensionless), and line strength (S in atomic units, where 1 a.u. = 6.460×10^{-36} $cm^2 \cdot esu^2$), are interrelated and connected with each other.

For E1, E2, M1, and M2 transitions, A value (in unit s^{-1}) can be obtained in terms of line strength S (in unit a.u.), and the transition wavelength λ (in unit Å),[59]

$$A(\text{E1}) = \frac{2.02613 \times 10^{18}}{(2J+1)\lambda^3} S(\text{E1}),$$

$$A(\text{M1}) = \frac{2.69735 \times 10^{13}}{(2J+1)\lambda^3} S(\text{M1}),$$

$$A(\mathrm{E2}) = \frac{1.11995\times10^{18}}{(2J+1)\lambda^5}S(\mathrm{E2}),$$
$$A(\mathrm{M2}) = \frac{1.49097\times10^{13}}{(2J+1)\lambda^5}S(\mathrm{M2}). \quad (2)$$

Furthermore, the oscillator strength f_{ij} (dimensionless) and the line strength S (in unit a.u.) are related by the following standard equations[60]

$$f_{ij}(\mathrm{E1}) = \frac{303.75}{\lambda g_i}S(\mathrm{E1}), \quad f_{ij}(\mathrm{M1}) = \frac{4.044\times10^{-3}}{\lambda g_i}S(\mathrm{M1}),$$
$$f_{ij}(\mathrm{E2}) = \frac{167.89}{\lambda^3 g_i}S(\mathrm{E2}), \quad f_{ij}(\mathrm{M2}) = \frac{2.236\times10^{-3}}{\lambda^3 g_i}S(\mathrm{M2}), \quad (3)$$

where g_i and g_j are the statistical weights of the lower i and upper j levels, respectively.

To further make uncertainty (or accuracy) estimates of the present MCDHF and RMBPT radiative transition rates (or A values), following Fischer[61] and Ekman *et al.*,[62] we define the relative deviation $\mathrm{d}T$ as the percentage differences (%) between the two A values (A_1 and A_2) for a same transition:

$$\mathrm{d}T = \frac{|A_1 - A_2|}{\max(A_1, A_2)}. \quad (4)$$

The $\mathrm{d}T$ value ranges from 0 to 1, a $\mathrm{d}T$ value closer to 0 indicates a higher degree of similarity between the two A values, $\mathrm{d}T = 0$ means the two A values are identical. Conversely, a $\mathrm{d}T$ value farther from 0 indicates greater discrepancies between the two.

To calculate the lifetime (τ) of an excited level j, one can use the A values as follows:[7]

$$\tau_j = \frac{1}{\sum_i A_{ij}}, \quad (5)$$

where i represents all the lower levels that can be accessed from the excited level j. In this study, the lifetime calculation does not differentiate between transition types, considering both allowed E1 transitions and forbidden M1, M2, and E2 transitions, although our research indicates that forbidden transitions have a negligible effect on lifetimes of the $n \leq 6$ levels, contributing at most 0.6%.

3. Results and discussion

3.1. Energies

In Table 1, using both the MCDHF and RMBPT methods, we present the energies of the 35 lowest levels from $(1s^2)nl$ configurations with $n \leq 6$ for Ge XXX. This table also includes previous theoretical results from Liang and Badnell,[15] Zhang *et al.*,[42] Johnson *et al.*,[43] and Vainshtain and Safronova,[41] as well as experimental data from NIST.[45] In Table 1, we also provide the lifetimes for the levels with $n \leq 6$. A detailed discussion of these lifetimes will be included in Subsection 3.3.

To better illustrate the accuracy of the energies from the current MCDHF calculations, in Fig. 1, we compare the results with various theoretical and experimental data. Additionally, we also include MCDHF results from Khatri *et al.*[44] in the figure, which are not listed in Table 1 due to space constraints. For clarity, we adjust the original energy ratios for Key=2 (i.e., $2p_{1/2}$) from Khatri *et al.*[44] by subtracting 0.0006 and for Key=3 (i.e., $2p_{3/2}$) from Liang and Badnell[15] by adding 0.006.

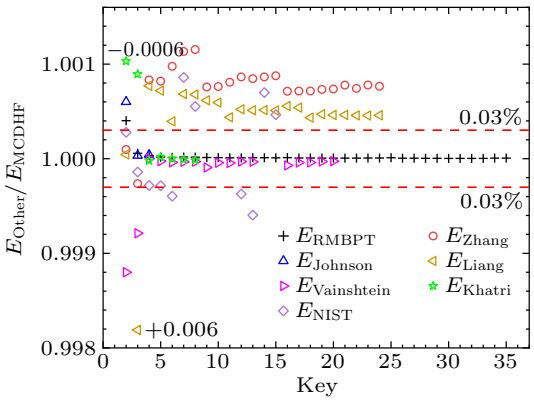


Fig. 1. Comparisons of energies with those from the present MCDHF calculations (E_{MCDHF}) for the $(1s^2)nl$ levels with $n \leq 6$ in Ge XXX. The other energies include present RMBPT ones (E_{RMBPT}), along with theoretical results from Zhang *et al.* (E_{Zhang}),[42] Johnson *et al.* (E_{Johnson}),[43] Liang and Badnell (E_{Liang}),[15] Vainshtain and Safronova ($E_{\mathrm{Vainshtain}}$),[41] and Khatri *et al.* (E_{Khatri}),[44] and compiled experimental data from NIST (E_{NIST}).[45] The horizontal coordinate "Key" is defined in Table 1. For clarity, we adjust the original energy ratios for Key = 2 (i.e., $2p_{1/2}$) from Khatri *et al.*[44] by subtracting 0.0006 and for Key = 3 (i.e., $2p_{3/2}$) from Liang and Badnell[15] by adding 0.006. The two horizontal dashed lines indicate relative differences of ±0.03%.

From Table 1 and Fig. 1, it can be seen firstly that the energies of levels with $n \leq 6$ from both present MCDHF and RMBPT methods are highly consistent, with all energies matching within 0.006%. The energy for $2p_{1/2}$ shows a slightly larger deviation, but still falls within 0.04%. Furthermore, As atomic number Z increases, both the effects of relativistic and QED corrections become more significant.[63] For Ge XXX, there are only two highly accurate experimental energies available, i.e., the $2p_{1/2}$ and $2p_{3/2}$ levels, which will be described in detail in the following paragragh. As shown in Table 1, for the two levels, the agreements between the results from the present two methods (MCDHF and RMBPT) and the NIST experimental values[45] are similar, indicating that dealing with the QED and relativistic effects, the present two methods are comparable.

Secondly, NIST[45] provides experimental energy values for 11 levels. The energies for $2p_{1/2}$ and $2p_{3/2}$ come from the measurements of tokamak discharge by Hinnov *et al.*,[21] which have very high precision, with uncertainties of ±25 cm^{-1} and ±140 cm^{-1}, respectively. The remaining 9 energies for 3s, 3p, 3d, 4d, and 4f levels are derived from laser-produced plasma measurements by Behring *et al.*,[64]

with a large uncertainty of ± 30000 cm^{-1}. Overall, compared to our MCDHF results, the experimental values are either higher or lower, with no significant systematic bias observed. The experimentally high-precision energies for $2p_{1/2}$ and $2p_{3/2}$ match our MCDHF results very well, both within 0.03%. Among the 9 lower-precision experimental levels, four match our results within 0.03%–0.04%, and five within 0.05%–0.09%. These five levels are: $3d_{3/2}$, $3d_{5/2}$, $4d_{5/2}$, $4f_{5/2}$, and $4f_{7/2}$. We believe the precision of the five NIST experimental levels may be limited, therefore we call for high-precision experimental or/and theoretical work to further verify these results.

Table 1. Energies (E, in unit eV) and lifetimes (τ, in unit s) of $(1s^2)nl$ levels with $n \leq 6$ for Ge XXX. "Key", "Con.", and "j" are the index, configuration, and total angular momentum of a level, respectively. Energies include present MCDHF ($E_{\rm MCDHF}$) and RMBPT ($E_{\rm RMBPT}$) methods, along with theoretical results from Liang and Badnell ($E_{\rm Liang}$),[15] Zhang *et al.* ($E_{\rm Zhang}$),[42] Johnson *et al.* ($E_{\rm Johnson}$),[43] Vainshtain and Safronova ($E_{\rm Vainshtein}$),[41] and compiled experimental data from NIST ($E_{\rm NIST}$).[45] Additionally, we have included the lifetimes of these energy levels calculated using the present length gauge radiative rates (A values) from MCDHF and RMBPT methods in Table 2, denoted as $\tau_{\rm MCDHF}$ and $\tau_{\rm RMBPT}$, respectively. $\tau_{\rm Liang}$ represents the lifetimes derived from the A values reported by Liang and Badnell.[15]

Key	Con.	j	$E_{\rm MCDHF}$	$E_{\rm RMBPT}$	$E_{\rm Liang}$	$E_{\rm Zhang}$	$E_{\rm Johnson}$	$E_{\rm Vainshtein}$	$E_{\rm NIST}$	$\tau_{\rm MCDHF}$	$\tau_{\rm RMBPT}$	$\tau_{\rm Liang}$
1	2s	1/2	0.0000	0.0000	0.0000	0.000	0.0000	0.000	0.0000	⋯	⋯	⋯
2	2p	1/2	61.8850	61.9098	61.8878	61.891	61.9222	61.8107	61.9023	4.23–10	4.23–10	4.17–10
3	2p	3/2	101.057	101.062	100.267	101.03	101.060	100.977	101.0425	9.49–11	9.49–11	9.71–11
4	3s	1/2	1792.71	1792.76	1794.09	1794.2	1792.78	1792.71	1792.2	1.47–13	1.47–13	1.57–13
5	3p	1/2	1809.92	1809.95	1811.22	1811.4	⋯	1809.87	1809.4	5.37–14	5.38–14	5.52–14
6	3p	3/2	1821.52	1821.55	1822.24	1823.3	⋯	1821.45	1820.8	5.66–14	5.66–14	5.74–14
7	3d	3/2	1827.93	1827.96	1829.18	1830.0	⋯	1827.87	1829.5	1.86–14	1.86–14	1.86–14
8	3d	5/2	1831.59	1831.62	1832.83	1833.7	⋯	1831.53	1832.6	1.89–14	1.89–14	1.88–14
9	4s	1/2	2411.27	2411.30	2412.76	2413.1	⋯	2411.05	⋯	2.17–13	2.17–13	2.50–13
10	4p	1/2	2418.36	2418.38	2419.79	2420.2	⋯	2418.25	⋯	9.16–14	9.15–14	1.00–13
11	4p	3/2	2423.24	2423.26	2424.30	2425.2	⋯	2423.13	⋯	9.56–14	9.55–14	1.01–13
12	4d	3/2	2425.90	2425.93	2427.17	2428.0	⋯	2425.83	2425	4.31–14	4.31–14	4.40–14
13	4d	5/2	2427.45	2427.47	2428.69	2429.5	⋯	2427.37	2426	4.40–14	4.39–14	4.41–14
14	4f	5/2	2427.60	2427.63	2428.85	2429.7	⋯	⋯	2429.3	8.86–14	8.86–14	8.85–14
15	4f	7/2	2428.37	2428.39	2429.61	2430.5	⋯	⋯	2429.5	8.91–14	8.91–14	8.89–14
16	5s	1/2	2695.28	2695.31	2696.78	2697.2	⋯	2695.09	⋯	3.43–13	3.43–13	4.89–13
17	5p	1/2	2698.87	2698.89	2700.33	2700.8	⋯	2698.76	⋯	1.56–13	1.56–13	2.01–13
18	5p	3/2	2701.37	2701.39	2702.54	2703.3	⋯	2701.26	⋯	1.62–13	1.62–13	1.97–13
19	5d	3/2	2702.72	2702.74	2703.99	2704.7	⋯	2702.64	⋯	8.28–14	8.27–14	9.07–14
20	5d	5/2	2703.51	2703.53	2704.76	2705.5	⋯	2703.44	⋯	8.46–14	8.44–14	8.76–14
21	5f	5/2	2703.60	2703.61	2704.85	2705.7	⋯	⋯	⋯	1.71–13	1.71–13	1.73–13
22	5f	7/2	2703.99	2704.01	2705.23	2706.0	⋯	⋯	⋯	1.72–13	1.72–13	1.73–13
23	5g	7/2	2703.99	2704.01	2705.23	2706.1	⋯	⋯	⋯	2.89–13	2.88–13	2.89–13
24	5g	9/2	2704.23	2704.25	2705.47	2706.3	⋯	⋯	⋯	2.89–13	2.89–13	2.90–13
25	6s	1/2	2848.76	2848.79	⋯	⋯	⋯	⋯	⋯	5.26–13	5.25–13	⋯
26	6p	1/2	2850.83	2850.84	⋯	⋯	⋯	⋯	⋯	2.50–13	2.49–13	⋯
27	6p	3/2	2852.27	2852.28	⋯	⋯	⋯	⋯	⋯	2.59–13	2.58–13	⋯
28	6d	3/2	2853.05	2853.06	⋯	⋯	⋯	⋯	⋯	1.41–13	1.41–13	⋯
29	6d	5/2	2853.50	2853.52	⋯	⋯	⋯	⋯	⋯	1.44–13	1.44–13	⋯
30	6f	5/2	2853.56	2853.57	⋯	⋯	⋯	⋯	⋯	2.92–13	2.91–13	⋯
31	6f	7/2	2853.79	2853.79	⋯	⋯	⋯	⋯	⋯	2.94–13	2.92–13	⋯
32	6g	7/2	2853.79	2853.80	⋯	⋯	⋯	⋯	⋯	4.95–13	4.93–13	⋯
33	6g	9/2	2853.92	2853.93	⋯	⋯	⋯	⋯	⋯	4.96–13	4.94–13	⋯
34	6h	9/2	2853.92	2853.94	⋯	⋯	⋯	⋯	⋯	7.48–13	7.47–13	⋯
35	6h	11/2	2854.01	2854.03	⋯	⋯	⋯	⋯	⋯	7.49–13	7.48–13	⋯

Thirdly, although the energy values of our MCDHF two 2p levels match the NIST[45] experimental ones very well, both within 0.03% as mentioned above. However, given that the energy values of the 2p levels (below 101 eV) are significantly lower than those of other higher levels with $n \geq 3$ (above 1790 eV), their relative deviations can be easily influenced by electron correlation energies and other factors. Consequently, large relatively deviations between different theoretical calculations are often observed. For example, for the $2p_{1/2}$ level, the energy differences between our MCDHF results and those from Johnson *et al.*[43] (third-order perturbation theory), Khatri *et al.*[44] (MCDHF), and Vainshtein and Safronova[41] (semi-empirical extrapolation method) are 0.06%, 0.16%, and 0.12%, respectively. And for the $2p_{3/2}$ level, the energy differences between our MCDHF results and those from Khatri *et al.*,[44] Vainshtein and Safronova,[41] and Liang and Badnell[15] (semi-relativistic approach) are 0.09%, 0.08%, and 0.8%, respectively. However, we also observe in

Fig. 1 that the energy values for the two 2p levels from Zhang *et al.*[42] agree very well with our MCDHF results, which is surprising, since their calculations did not account for neither Breit or QED effects. We speculate that this good agreement is likely because Zhang *et al.*[42] optimized the two values based on highly accurate experimental data. Our RMBPT test calculations show that ignoring both Breit and QED effects would result in a decrease of 0.04% for the $2p_{1/2}$ level and an increase of 1.1% for the $2p_{3/2}$ level, while energy values for other high levels with $n = 3$–6 would increase by 0.07% to 0.11%.

At last, for high levels with $n \geq 3$, neglecting both Breit and QED effects leads to a systematic increase in energy values by 0.07% to 0.11%, as noted above, This effect is clearly visible when comparing the energy values of Zhang *et al.*[42] with our MCDHF results. Additionally, the results of Liang and Badnell[15] shows a systematic increase of 0.04% to 0.08% compared to our MCDHF energies, primarily due to the neglect of QED effects. Our RMBPT test calculations also indicate that ignoring QED effects results in a systematic increase in energy values by 0.03% to 0.06% for high levels with $n = 3$–6. We note here that though the energies from Liang and Badnell[15] are generally consistent with the NIST experimental data,[45] however, they exhibit somewhat less precision. For example, the discrepancy between the results from Liang and Badnell[15] and the NIST data is about 0.8% for the $2p_{3/2}$ level, the difference between our MCDHF results and the NIST data is only within 0.02% for the same level. This indicates that the accuracy of our MCDHF energies has improved by over an order of magnitude compared to Liang and Badnell ones.[15] Furthermore, Vainshtain and Safronova[41] provided energy values for 15 levels with $n = 3$–5 that are consistent with our MCDHF results, with discrepancies within 0.01%. It is worth mentioning that Vainshtain and Safronova[41] did not report any energies for the 4f, 5f, and 5g levels.

In short, we have obtained two sets of mutually consistent and highly accurate energy levels, which confirms the accuracy of our wavefunctions. We then use these accurate wavefunctions to calculate radiative rates.

3.2. Radiative rates

In Table 2, we present the length gauge transition properties for lithium-like germanium (Ge XXX) obtained from both the present MCDHF and RMBPT methods. The transition properties include transition wavelength λ in unit Å), radiative transition rate (A value in unit s^{-1}), absorption oscillator strength (f, dimensionless), and line strength in atomic units (S in a.u., 1 a.u. $= 6.460 \times 10^{-36}$ $cm^2 \cdot esu^2$). We provides results for various types of transitions in the table, including dipole-allowed (E1) transitions and dipole-forbidden transitions (magnetic dipole M1, magnetic quadrupole M2, and electric quadrupole E2).

To further make uncertainty (or accuracy) estimates of the present MCDHF and RMBPT radiative transition rates (or A values). In Table 2, we also provide dT values (defined in Eq. (4)). The dT value ranges from 0 to 1, a dT value closer to 0 indicates a higher degree of similarity between the two A values, d$T = 0$ means the two A values are identical. Conversely, a dT value farther from 0 indicates greater discrepancies between the two. Here, dT_1 denotes the relative deviations of the length gauge results from both the present MCDHF and RMBPT methods, while dT_2 represents the relative deviations between the length and velocity gauges ones from the present MCDHF calculations.

To provide a clearer illustration of the accuracy estimates of the present MCDHF and RMBPT A values, In Figs. 2(a)–2(d), we show how the dT values for E1, E2, M1, and M2 transitions vary with changes in the A values from the present MCDHF length gauge calculations ($A_{\rm MCDHF}$).

In Fig 2, we show the consistency of the A values for strong transitions obtained from both the present MCDHF and RMBPT length gauges. Additionally, the results from the MCDHF length gauge and velocity gauge are also in agreement. For easily description in the following, we define a transition as strong if its radiative rate exceeds 0.01% of the maximum radiative rate for that type of transition.

From Table 2 and Fig 2, we can obtain as following: Firstly, for 127 strong E1 transitions (with the strongest being $2p_{3/2}$–$3d_{5/2}$, having a radiative rate of 5.286×10^{13} s^{-1}), 113 and 125 transitions have dT_1 values less than 1.0% and 3.0%, respectively. Only two transitions, $4f_{5/2}$–$6d_{3/2}$ and $4f_{7/2}$–$6d_{5/2}$, exhibit slightly larger dT_1 values, both around 5%. For these 127 strong transitions, dT_2 values are all below 1%, indicating that the present MCDHF A values are slightly more accurate compared to the RMBPT ones.

Secondly, for 123 strong E2 transitions (the strongest E2 transition being $2s_{1/2}$–$3d_{5/2}$, which has a A value of 4.517×10^{10} s^{-1}), 108 and 120 transitions have dT_1 values less than 2.0% and 5.0%, respectively. Only three transitions, $4f_{5/2}$–$6p_{1/2}$, $4f_{7/2}$–$6p_{3/2}$, and $2p_{1/2}$–$6p_{3/2}$, exhibit slightly larger dT_1 values of 5%, 6%, and 7%, respectively. For these 123 strong transitions, dT_2 values are below 1% for 120 transitions and below 2.5% for 122 transitions. Only one transition, $2p_{1/2}$–$6p_{3/2}$, has a slightly larger dT_2 value of 5.1%.

Thirdly, for 41 strong M1 transitions (with the strongest M1 transition being $2p_{3/2}$–$3p_{1/2}$, which has a A value of 8.529×10^{6} s^{-1}), 28 and 37 transitions have dT_1 values are below 2.0% and 4.0%, respectively. Only two transitions, $4d_{5/2}$–$6d_{3/2}$ and $4d_{3/2}$–$6d_{5/2}$, show larger dT_1 values, being 13% and 19%, respectively. Both the two transitions are relatively weak, being only 0.04% and 0.01% of the A value of the strongest M1 transition, respectively.

Table 2. Length gauge transition properties of different types ("Type") for Ge XXX, including both dipole-allowed (E1) and dipole-forbidden transitions (magnetic dipole M1, magnetic quadrupole M2, and electric quadrupole E2), from both the present MCDHF and RMBPT methods. "i" and "j" are the lower and upper levels of a transition, which are defined as the "Key" in Table 1, λ is transition wavelength (in unit Å), A is radiative transition rate (in unit s^{-1}), f is absorption oscillator strength (dimensionless), S is line strength in atomic unit (in unit a.u., 1 a.u. = 6.460×10^{-36} $cm^2\cdot esu^2$). Furthermore, dT (in %, defined in Eq. (4)) represents the relative deviations between the two sets of radiative rates (A values), expressed as a percentage (%), and dT_1 denotes the results between the present MCDHF and RMBPT length gauge ones, while dT_2 indicates those between the length and velocity gauge A values from the present MCDHF method. Additionally, $a\pm b\equiv a\times10^{\pm b}$. Note: Only a subset of transition data are presented here, the complete datasets are openly available in Science Data Bank at https://doi.org/10.57760/sciencedb.j00113.00135.

i	j	Type	$\lambda_{\rm MCDHF}$	$\lambda_{\rm RMBPT}$	$A_{\rm MCDHF}$	$f_{\rm MCDHF}$	$S_{\rm MCDHF}$	$A_{\rm RMBPT}$	$f_{\rm RMBPT}$	$S_{\rm RMBPT}$	dT_1 (%)	dT_2 (%)
1	2	E1	2.0035+02	2.0027+02	2.363+09	1.422−02	1.875−02	2.365+09	1.422−02	1.875−02	0.11	2.52
1	3	E1	1.2269+02	1.2268+02	1.054+10	4.757−02	3.843−02	1.054+10	4.757−02	3.842−02	0.01	0.70
1	3	M2	1.2269+02	1.2268+02	7.733+01	3.490−10	5.767−01	7.735+01	3.490−10	5.767−01	0.02	…
1	5	E1	6.8503+00	6.8501+00	1.859+13	1.308−01	5.897−03	1.858+13	1.307−01	5.896−03	0.02	0.28
1	6	E1	6.8066+00	6.8065+00	1.765+13	2.452−01	1.099−02	1.765+13	2.452−01	1.099−02	0.01	0.26
1	6	M2	6.8066+00	6.8065+00	4.207+07	5.844−07	1.649−01	4.207+07	5.844−07	1.649−01	0.01	…
1	7	M1	6.7828+00	6.7827+00	7.895+04	1.089−09	3.653−06	7.821+04	1.079−09	3.619−06	0.94	…
1	7	E2	6.7828+00	6.7827+00	4.485+10	6.187−04	2.300−03	4.485+10	6.186−04	2.299−03	0.00	0.12
1	8	E2	6.7692+00	6.7691+00	4.517+10	9.310−04	3.440−03	4.517+10	9.309−04	3.439−03	0.00	0.12
1	10	E1	5.1268+00	5.1267+00	8.113+12	3.197−02	1.079−03	8.114+12	3.197−02	1.079−03	0.01	0.29
1	11	E1	5.1165+00	5.1164+00	7.838+12	6.153−02	2.073−03	7.841+12	6.155−02	2.073−03	0.04	0.24
1	11	M2	5.1165+00	5.1164+00	3.299+07	2.590−07	3.104−02	3.301+07	2.591−07	3.105−02	0.04	…
1	12	M1	5.1109+00	5.1108+00	4.612+04	3.612−10	9.131−07	4.583+04	3.589−10	9.073−07	0.64	…
1	12	E2	5.1109+00	5.1108+00	5.861+09	4.591−05	7.300−05	5.862+09	4.591−05	7.301−05	0.01	0.09
1	13	E2	5.1076+00	5.1075+00	6.082+09	7.136−05	1.133−04	6.083+09	7.137−05	1.133−04	0.01	0.09
1	14	M2	5.1073+00	5.1072+00	5.155+01	6.048−13	7.209−08	5.094+01	5.976−13	7.123−08	1.18	…
1	17	E1	4.5939+00	4.5939+00	4.166+12	1.318−02	3.987−04	4.168+12	1.319−02	3.989−04	0.06	0.29
1	18	E1	4.5897+00	4.5896+00	4.051+12	2.559−02	7.733−04	4.056+12	2.562−02	7.742−04	0.13	0.24
1	18	M2	4.5897+00	4.5896+00	2.117+07	1.337−07	1.157−02	2.120+07	1.339−07	1.158−02	0.13	…
1	19	M1	4.5874+00	4.5874+00	2.599+04	1.640−10	3.721−07	2.592+04	1.635−10	3.710−07	0.29	…
1	19	E2	4.5874+00	4.5874+00	1.429+09	9.014−06	1.037−05	1.429+09	9.015−06	1.037−05	0.01	0.04
1	20	E2	4.5860+00	4.5860+00	1.522+09	1.440−05	1.654−05	1.522+09	1.440−05	1.654−05	0.01	0.03
1	21	M2	4.5859+00	4.5859+00	4.475+01	4.233−13	3.652−08	4.423+01	4.184−13	3.610−08	1.16	…
1	26	E1	4.3491+00	4.3490+00	2.410+12	6.834−03	1.957−04	2.411+12	6.838−03	1.958−04	0.06	0.28
1	27	E1	4.3469+00	4.3468+00	2.351+12	1.332−02	3.812−04	2.355+12	1.334−02	3.819−04	0.18	0.22
1	27	M2	4.3469+00	4.3468+00	1.369+07	7.756−08	5.700−03	1.371+07	7.770−08	5.710−03	0.18	…
1	28	M1	4.3457+00	4.3457+00	1.565+04	8.862−11	1.905−07	1.567+04	8.874−11	1.907−07	0.14	…
1	28	E2	4.3457+00	4.3457+00	4.970+08	2.814−06	2.751−06	4.951+08	2.804−06	2.741−06	0.38	0.34
1	29	E2	4.3450+00	4.3450+00	5.422+08	4.604−06	4.498−06	5.403+08	4.588−06	4.483−06	0.34	0.33
1	30	M2	4.3449+00	4.3449+00	3.281+01	2.786−13	2.045−08	3.211+01	2.726−13	2.001−08	2.16	…
⋮	⋮	⋮	⋮	⋮	⋮	⋮	⋮	⋮	⋮	⋮	⋮	⋮

And fourthly, for 74 strong M2 transitions (the strongest M2 transition being $2p_{3/2}$–$3d_{5/2}$, which has a radiative rate of 1.471×10^8 s^{-1}), there are 71 transitions having dT_1 values less than 0.8%, and all less than 2.2%.

In Fig. 3, we compare our MCDHF length gauge A values of E1 transition with our RMBPT length gauge ones, and with previous theoretical results. The well consistency between our two length gauge MCDHF and RMBPT A values has been discussed on dT values in detail above, so we will not repeat here.

As shown in Fig. 3, our MCDHF results align very well with existing fully relativistic results. Specifically, our MCDHF A values agree with those from Johnson *et al.*[43] (third-order many-body perturbation theory) within 0.4%, with Khatri *et al.*[44] (MCDHF) within 0.6%, and with Zhang *et al.*[42] (fully relativistic) within 3%. However, Liang and Badnell[15] present E1 transition radiative rates for 92 transitions between levels with $n\leq5$ that show significant discrepancies compared to our MCDHF results. Notably, there are 60, 43, and 25 transitions where the differences exceed 2%, 5%, and 10%, respectively. There are 12 transitions having discrepancies greater than 22%. Specifically, 8 of these are strong transitions: $2p_{1/2}$–$5s_{1/2}$, $3p_{1/2}$–$5s_{1/2}$, $2p_{3/2}$–$5s_{1/2}$, $2p_{1/2}$–$4s_{1/2}$, $2s_{1/2}$–$5p_{1/2}$, $2s_{1/2}$–$5p_{3/2}$, $3d_{3/2}$–$5p_{1/2}$, $3d_{3/2}$–$5p_{3/2}$. For these 8 strong transitions, Liang and Badnell[15] reported A values that are consistently lower than our MCDHF results by a factor ranging from 0.28 to 0.69. These discrepancies are primarily due to differences in the line strengths (S). Additionally, there are 4 weak transitions with $\Delta n=0$: $3p_{3/2}$–$3d_{3/2}$, $4p_{3/2}$–$4d_{3/2}$, $5p_{3/2}$–$5d_{3/2}$, and $5f_{7/2}$–$5g_{7/2}$. The A value for the $5f_{7/2}$–$5g_{7/2}$ transition reported by Liang and Badnell[15] shows the largest discrepancy, being only 0.05 times our MCDHF value (this transition is not shown in the

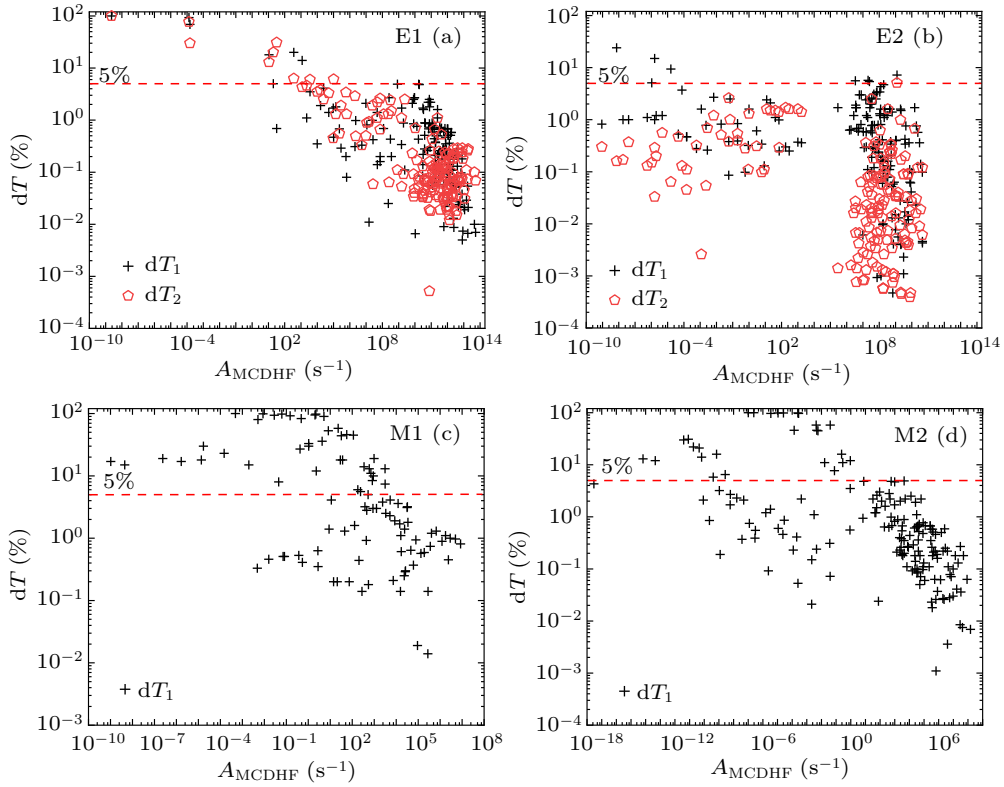


Fig. 2. The relationship between the relative deviations dT (in %, defined in Eq. (4)) of radiative rates (A values) and the present MCDHF length gauge A values ($A_{\rm MCDHF}$), and dT_1 denotes the results between the present MCDHF and RMBPT length gauge ones, while dT_2 indicates those between the length and velocity gauge A values from the present MCDHF method. (a) for E1, (b) for E2, (c) for M1, and (d) for M2 transitions. The horizontal dashed line represents relative differences of 5%.

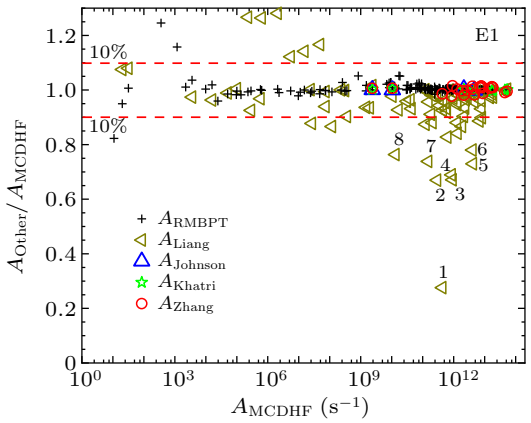


Fig. 3. Comparisons of other theoretical A values with the present MCDHF length gauge ones ($A_{\rm MCDHF}$) of E1 transition. Here, other theoretical A values are from the present RMBPT length gauge ones ($A_{\rm RMBPT}$), as well as from calculations by Liang and Badnell ($A_{\rm Liang}$)[15], Johnson *et al.* ($A_{\rm Johnson}$),[43] Khatri *et al.* ($A_{\rm Khatri}$),[44] and Zhang *et al.* ($A_{\rm Zhang}$),[42] respectively. The numbers near the small triangles correspond to the following transitions, 1: $2p_{1/2}$–$5s_{1/2}$, 2: $3p_{1/2}$–$5s_{1/2}$, 3: $2p_{3/2}$–$5s_{1/2}$, 4: $2p_{1/2}$–$4s_{1/2}$, 5: $2s_{1/2}$–$5p_{1/2}$, 6: $2s_{1/2}$–$5p_{3/2}$, 7: $3d_{3/2}$–$5p_{1/2}$, 8: $3d_{3/2}$–$5p_{3/2}$. The data between the two horizontal red dashed lines indicate that the agreement is within 10%.

figure due to its very small rate, below 0.001 s^{-1}). The differences for these 4 $\Delta n = 0$ weak transitions are primarily due to differences in the wavelengths. The poorer agreement of high-Z transition properties between the semi-relativistic results from Liang and Badnell[15] and the fully relativistic results from Zhang *et al.*[42] have been highlighted in their own paper.[15] Specifically, only about 57% of the available transitions for Kr XXXIV, which is close to Ge XXX in the lithium-like sequence, agree within 10% with the fully relativistic results of Zhang *et al.*[42] The significant discrepancy of the A values between those from Liang and Badnell[15] and our fully relativistic MCDHF ones is likely due to their using of a semi-relativistic approach and limited consideration of electron correlation. Our recent study on lithium-like iron[7] demonstrates that the electron correlation alone can affect the A values by up to approximately 60% and the level lifetimes by up to around 20%. In fact, even for lithium-like iron, it is crucial to incorporate relativistic effects right from the beginning,[7] not to mention for Ge XXX. We note here that Liang and Badnell[15] also provided semi-relativistic A values for forbidden transitions (E2, M1, M2), and the agreement with our MCDHF ones is similar to that for E1 transitions.

In short, our two theoretical A values are self-consistent and align with existing fully relativistic ones. However, semi-relativistic results of Liang and Badnell[15] introduce significant deviations for A values of Ge XXX, which in turn could lead to greater uncertainties in the lifetimes.

3.3. Lifetimes

From Table 1 and Fig 4, we can see that the length gauge lifetimes from two sets of present MCDHF and RMBPT methods agree well with each other. For example, all of the $n \leq 5$ and $n \leq 6$ lifetimes are within 0.2% and 0.6%, respectively.

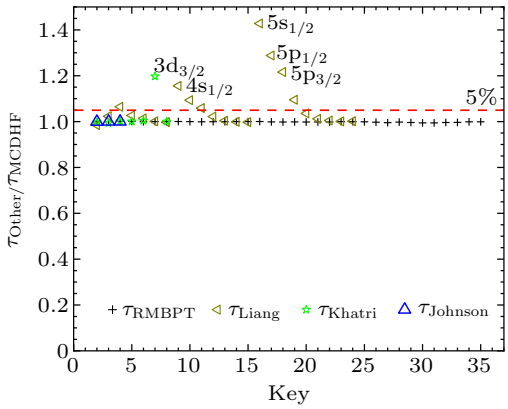


Fig. 4. Comparisons of other theoretical lifetimes ($\tau_{\rm Other}$) with the present MCDHF length gauge ones ($\tau_{\rm MCDHF}$). Here, other theoretical lifetimes are derived from the present RMBPT length gauge A values ($\tau_{\rm RMBPT}$), as well as from A values calculated by Liang and Badnell ($\tau_{\rm Liang}$),[15] Khatri *et al.* ($\tau_{\rm Khatri}$),[44] and Johnson *et al.* ($\tau_{\rm Johnson}$),[43] respectively. The horizontal dashed line represents relative differences of 5%.

We can also see that the three lifetimes derived from the third-order many-body perturbation theory A values of Johnson *et al.*[43] are consistent with the present MCDHF results, all within 0.1%. The seven lifetimes derived from Khatri *et al.*'s MCDHF A values[44] align closely with our current MCDHF findings, falling within a 0.4% margin of difference for all levels, except for the $3d_{3/2}$ level. In this specific case, the lifetime discrepancy reaches 20%, primarily because Khatri *et al.*[44] did not report the A value for the $2p_{3/2}$–$3d_{3/2}$ transition. Both our present MCDHF and RMBPT findings indicate that the A value for this transition is approximately 0.2 times smaller than the dominant decay channel (i.e., the $2p_{1/2}$–$3d_{3/2}$ transition) from the upper level $3d_{3/2}$. Due to space constraints in Table 1, the lifetimes derived from the A values reported by Johnson *et al.*[43] and Khatri *et al.*[44] are not included in the table.

Furthermore, the 23 lifetimes derived from the autostructure A values reported by Liang and Badnell[15] exhibit significant discrepancies compared to our current MCDHF ones. Most differences exceed 2%, with 8 lifetimes differing by more than 6% and 4 lifetimes differing by over 15%, specifically for the $4s_{1/2}$, $5p_{3/2}$, $5p_{1/2}$, and $5s_{1/2}$ levels. Liang and Badnell's lifetimes are higher than our MCDHF results by 16%, 22%, 29%, and 43%, respectively. Since lifetimes are directly related to the radiative rates, as shown in Eq. (5), substantial differences in the radiative rates can result in significant variations in the lifetimes.

In short, we provide two sets of highly consistent fully relativistic $n \leq 6$ lifetime values. Additionally, to the best of our knowledge, there are currently no experimental lifetimes of Ge XXX. We call for future experimental efforts in this area.

4. Conclusion

Employing two fully relativistic methods: the multi-reference configuration Dirac–Hartree–Fock (MCDHF) method implemented in the GRASP2K code (version 2018) and the relativistic many-body perturbation theory (RMBPT) implemented in the FAC code, we provide energies, radiative properties, and lifetimes for the lowest 35 energy levels from $1s^2nl$ configurations (with $n \leq 6$ and $l \leq n-1$) of Ge XXX. The radiative properties include transition wavelengths, radiative rates, absorption oscillator strengths, and line strengths for both allowed (E1) and forbidden transitions (magnetic dipole M1, magnetic quadrupole M2, and electric quadrupole E2). We consider the Breit interactions, the leading QED effects (vacuum polarization and self-energy), and detailed electron correlation effects. Therefore, the present work provides more accurate and complete theoretical results for Ge XXX, which can serve as benchmark data for future experimental measurements, and related plasma spectra diagnostics.

Data availability statement

The data that support the findings of this study are openly available in Science Data Bank at address https://doi.org/10.57760/sciencedb.j00113.00135.

Acknowledgements

The author (Shuang Li) would like to express his gratitude for the support received through the Visiting Researcher Program at Fudan University (C. Y. Chen's research group) and the Institute of Applied Physics and Computational Mathematics (J. Yan's research group). The author (Shuang Li) would also like to express his gratitude to Yan Wang, Longfei Mu, and Siqi Wang for many valuable discussion in this research. Project supported by the Research Foundation for Higher Level Talents of West Anhui University (Grant No. WGKQ2021005).

References

[1] Ullmann J, Andelkovic Z and Brandau C, *et al.* 2017 *Nat. Commun.* **8** 15484
[2] Karr J P 2017 *Nat. Phys.* **13** 533
[3] Zhang G S, Deng B L, Yang J, Tang K, Meng B and Zhang X Q 2023 *At. Data Nucl. Data Tables* **149** 101547
[4] Skripnikov L V, Schmidt S, Ullmann J, Geppert C, Kraus F, Kresse B, Nortershauser W, Privalov A F, Scheibe B, Shabaev V M, Vogel M and Volotka A V 2018 *Phys. Rev. Lett.* **120** 093001
[5] Volotka A V, Glazov D A, Shabaev V M, Tupitsyn I I and Plunien G 2014 *Phys. Rev. Lett.* **112** 253004
[6] Yerokhin V A and Surzhykov A 2018 *J. Phys. Chem. Ref. Data* **47** 023105
[7] Li S, Zhao M, Liu G Q, Hu C B and Pan G Z 2023 *Chin. Phys. B* **32** 103101
[8] Liu X and Zhang J C 2023 *J. Korean Phys. Soc.* **82** 154
[9] Kumar P, Goyal A and Mohan M 2022 *Eur. Phys. J. Plus* **137** 1253
[10] Fontes C J and Zhang H L 2017 *At. Data Nucl. Data Tables* **113** 293
[11] Barzakh A, Andreyev A N, Raison C, *et al.* 2021 *Phys. Rev. Lett.* **127** 192501
[12] Deng B L, Jiang G and Zhang C Y 2014 *At. Data Nucl. Data Tables* **100** 1337

[13] Aggarwal K M and Keenan F P 2013 *At. Data Nucl. Data Tables* **99** 156

[14] Aggarwal K M and Keenan F P 2012 *At. Data Nucl. Data Tables* **98** 1003

[15] Liang G Y and Badnell N R 2011 *Astron. Astrophys.* **528** A69

[16] Namba S, Wang J H, Ohiro H, Zhang J W, Kishimoto M, Yamasaki K, Hasegawa N, Dinh T, Ishino M, Higashiguchi T and Nishikino M 2022 *Atoms* **10** 128

[17] Mitra-Kraev U and Del Zanna G 2019 *Astron. Astrophys.* **628** A134

[18] Neupert W M, Swartz M and Kastner S O 1973 *Sol. Phys.* **31** 171

[19] Boiko V, Faenov A and Pikuz S 1978 *J. Quantum Spectrosc. Radiat. Transfer* **19** 11

[20] Behring W E, Seely J F, Brown C M, Feldman U and Knauer J P 1989 *J. Opt. Soc. Am. B: Opt. Phys.* **6** 531

[21] Hinnov E, the TFTR Operating Team, Denne B and the JET Operating Team 1989 *Phys. Rev. A* **40** 4357

[22] Zhang W M, Zhang L, Cheng Y X, Morita S, Wang Z X, Hu A L, Zhang F L, Duan Y M, Zhou T F, Wang S X and Liu H Q 2022 *Phys. Scr.* **97** 045604

[23] Epp S W, López-Urrutia J R C, Brenner G, Mäckel V, Mokler P H, Treusch R, Kuhlmann M, Yurkov M V, Feldhaus J, Schneider J R, Wellhöfer M, Martins M, Wurth W and Ullrich J 2007 *Phys. Rev. Lett.* **98** 183001

[24] Chen H, Gu M F, Behar E, Brown G V, Kahn S M and Beiersdorfer P 2007 *Astrophys. J. Suppl. Ser.* **168** 319

[25] Yan Z C, Tambasco M and Drake G W F 1998 *Phys. Rev. A* **57** 1652

[26] Li W X, Amarsi A M, Papoulia A, Ekman J and Jönsson P 2021 *Mon. Not. R. Astron. Soc.* **502** 3780

[27] Zhang D H, Zhang F J, Ding X B and Dong C Z 2021 *Chin. Phys. B* **30** 043102

[28] Zeng J L, Li Y J and Yuan J M 2021 *J. Quantum Spectrosc. Radiat. Transfer* **272** 107777

[29] Liu X, Zhang J C and Wang Z W 2019 *Results Phys.* **12** 398

[30] Santana J A, Peña-Cotto E L, Butler E J M, Beiersdorfer P and Brown V G 2019 *Astrophys. J. Suppl. Ser.* **245** 9

[31] Santana J A, Lopez-Dauphin N A and Beiersdorfer P 2018 *Astrophys. J. Suppl. Ser.* **234** 13

[32] Santana J A, Lopez-Dauphin N A, Butler E J M and Beiersdorfer P 2018 *Astrophys. J. Suppl. Ser.* **238** 34

[33] Chen Z B, Wang K and Guo X L 2018 *J. Quantum Spectrosc. Radiat. Transfer* **220** 28

[34] El-Maaref A A 2016 *J. Quantum Spectrosc. Radiat. Transfer* **170** 45

[35] Hao L H, Liu J J and Kang X P 2016 *Eur. Phys. J. Plus* **131** 204

[36] Cai J, Yu W W and Zhang N 2014 *Chin. Phys. Lett.* **31** 093101

[37] Gu M F 2005 *At. Data Nucl. Data Tables* **89** 267

[38] Nahar S N and Pradhan A 1999 *Astron. Astrophys. Suppl. Ser.* **135** 347

[39] Fischer C F, Saparov M, Gaigalas G and Godefroid M 1998 *At. Data Nucl. Data Tables* **70** 119

[40] Kozhedub Y S, Volotka A V, Artemyev A N, Glazov D A, Plunien G, Shabaev V M, Tupitsyn I I and Stöhlker T 2010 *Phys. Rev. A* **81** 042513

[41] Vainshtein L A and Safronova U I 1985 *Phys. Scr.* **31** 519

[42] Zhang H L, Sampson D H and Fontes C J 1990 *At. Data Nucl. Data Tables* **44** 31

[43] Johnson W R, Liu Z W and Sapirstein J 1996 *At. Data Nucl. Data Tables* **64** 279

[44] Khatri I, Goyal A, Aggarwal S, Singh A K and Mohan M 2016 *Radiat. Phys. Chem.* **123** 46

[45] Kramida A, Ralchenko Y, Reader J and NIST ASD Team Online 2023 *NIST Atomic Spectra Database* (version 5.11). Accessed 19 July 2024

[46] Badnell N R 1986 *J. Phys. B: At. Mol. Phys.* **19** 3827

[47] Fischer C F, Gaigalas G, Jönsson P and Bieroń J 2019 *Comput. Phys. Commun.* **237** 184

[48] Gu M F 2008 *Can. J. Phys.* **86** 675

[49] Wang K, Si R, Dang W, Jönsson P, Guo X L, Li S, Chen Z B, Zhang H, Long F Y, Liu H T, Li D F, Hutton R, Chen C Y and Yan J 2016 *Astrophys. J. Suppl. Ser.* **223** 3

[50] Wang K, Jönsson P, Ekman J, Gaigalas G, Godefroid M R, Si R, Chen Z B, Li S, Chen C Y and Yan J 2017 *Astrophys. J. Suppl. Ser.* **229** 37

[51] Si R, Li S, Guo X L, Chen Z B, Brage T, Jönsson P, Wang K, Yan J, Chen C Y and Zou Y M 2016 *Astrophys. J. Suppl. Ser.* **227** 16

[52] Wang K, Chen Z B, Si R, Jönsson P, Ekman J, Guo X L, Li S, Long F Y, Dang W, Zhao X H, Hutton R, Chen C Y, Yan J and Yang X 2016 *Astrophys. J. Suppl. Ser.* **226** 14

[53] Fischer C F, Godefroid M, Brage T, Jönsson P and Gaigalas G 2016 *J. Phys. B: At. Mol. Opt. Phys.* **49** 182004

[54] Jönsson P, Godefroid M, Gaigalas G, Ekman J, Grumer J, Li W X, Li J G, Brage T, Grant I P, Bieroń J and Fischer C F 2022 *Atoms* **11** 7

[55] Jönsson P, Godefroid M, Gaigalas G, Ekman J, Grumer J, Li W X, Li J G, Brage T, Grant I P, Bieroń J and Fischer C F 2023 *Atoms* **11** 68

[56] Gu M F, Holczer T, Behar E and Kahn S 2006 *Astrophys. J.* **641** 1227

[57] Gu M F 2007 *Astrophys. J. Suppl. Ser.* **169** 154

[58] Lindgren I J 1974 *J. Phys. B: At. Mol. Opt. Phys.* **7** 2441

[59] Safronova U I, Safronova A S and Beiersdorfer P 2006 *J. Phys. B: At. Mol. Opt. Phys.* **39** 4491

[60] Aggarwal K M, Keenan F P and Lawson K D 2008 *At. Data Nucl. Data Tables* **94** 323

[61] Fischer C F 2009 *Phys. Scr.* **T134** 014019

[62] Ekman J, Godefroid M R and Hartman H 2014 *Atoms* **2** 215

[63] Wu C Q, Zhao R X, Zhang D H, Zhang M W, Xue Y L, Yu D Y, Dong C Z and Ding X B 2023 *Eur. Phys. J. D* **77** 129

[64] Behring W E, Seely J F, Brown C M, Feldman U and Knauer J P 1989 *J. Opt. Soc. Am. B: Opt. Phys.* **6** 531